Research in Astron. Astrophys. **2011** Vol. **11** No. **2**, 225–236
http://www.raa-journal.org *http://www.iop.org/journals/raa*

Research in Astronomy and Astrophysics

Numerical simulations of magnetic reconnection in the lower solar atmosphere *

Xiao-Yan Xu[1,2], Cheng Fang[2], Ming-De Ding[2] and Dan-Hui Gao[2]

[1] Purple Mountain Observatory, Chinese Academy of Science, Nanjing 210008, China; *xyxu@pmo.ac.cn*
[2] Department of Astronomy, Nanjing University, Nanjing 210093, China

Received 2009 November 23; accepted 2010 July 25

Abstract Observations indicate that Ellerman bombs (EBs) and chromospheric microflares both occur in the lower solar atmosphere, and share many common features, such as temperature enhancements, accompanying jet-like mass motions, short lifetime, and so on. These strongly suggest that EBs and chromospheric microflares could both probably be induced by magnetic reconnection in the lower solar atmosphere. With gravity, ionization and radiation considered, we perform two-dimensional numerical simulations of magnetic reconnection in the lower solar atmosphere. The influence of different parameters, such as intensity of the magnetic field and anomalous resistivity, on the results are investigated. Our result demonstrates that the temperature increases are mainly due to the joule dissipation caused by magnetic reconnection. The spectral profiles of EBs and chromospheric microflares are calculated with the non-LTE radiative transfer theory and compared with observations. It is found that the typical features of the two phenomena can be qualitatively reproduced.

Key words: Sun: chromosphere — Sun: photosphere — Sun: magnetic reconnection — Sun: numerical simulation

1 INTRODUCTION

Both Ellerman bombs (EBs) and chromospheric microflares are small short-lived solar eruptive events, which occur in the lower solar atmosphere, i.e. the photosphere and chromosphere. Owing to the simplicity of their structures, the study of the two phenomena can be very useful for understanding other eruptive processes and the mechanism of heating in the lower solar atmosphere. Recently, by using high resolution data, many authors investigated these processes in detail and found some new results on their properties and nature.

EBs, also well-known as moustaches, are small brightenings located in the lower solar chromosphere and upper photosphere. Observations indicate that the typical size of EBs is on the order of about one arcsecond (Zachariadis et al. 1987; Kurokawa et al. 1982; Denker 1997; Dara et al. 1997; Fang et al. 2006a), and the typical lifetime is about 10–20 min (Kurokawa et al. 1982; Nindos & Zirin 1998; Qiu et al. 2000; Fang et al. 2006a). Kitai (1983) and Kurokawa et al. (1982) detected an upward motion in these events with a velocity of about several kilometers per second. Dara et al.

∗ Supported by the National Natural Science Foundation of China.

(1997) found that a strong upward motion was related to strong EBs. On the other hand, Georgoulis et al. (2002) studied high spatial resolution data, which indicated that 80% of the EBs they studied showed downward photospheric motion at a velocity of 0.1–0.4 km s^{-1}. Fang et al. (2006a) used high-resolution spectral data of 14 EBs observed by the French-Italian 90 cm vacuum telescope, THEMIS, and found that the excess intensity in the two wings of both Hα and Ca II λ8542 is asymmetric. According to the semi-empirical models given by Fang et al. (2006a), the temperature enhancement in the photosphere and the lower chromosphere is about 600–1300 K. The total energy of the EBs is $10^{26} - 5\times10^{27}$ erg.

To explore the nature of EBs, it is important to study the relationship between EBs and ambient magnetic features. EBs are usually observed at the places close to sunspots or around strong magnetic structures (Zachariadis et al. 1987; Dara et al. 1997; Nindos & Zirin 1998). It was found that more than half of the EBs are located at or close to the magnetic polarity inversion lines, and the others are at the boundaries of unipolar magnetic areas (Qiu et al. 2000; Fang et al. 2006a). Georgoulis et al. (2002) found that EBs occur in the magnetic separatrix or quasi-separatrix layer of the lower chromosphere. Denker et al. (1995) found that EBs are often pushed away by expanding granules, so that one polarity magnetic feature may be driven to meet other opposite polarity features.

Based on observational results, several models of EBs have been proposed, but magnetic reconnection in the lower solar atmosphere is widely used to account for EBs (Hénoux et al. 1998; Ding et al. 1998; Georgoulis et al. 2002; Fang et al. 2003; Pariat et al. 2004; Fang et al. 2006a; Isobe et al. 2007). Using two-dimensional quasi-steady modeling, Litvinenko (1999) demonstrated that the magnetic reconnection in the lower solar atmosphere should be most efficient around the region of temperature minimum. Pariat et al. (2004) proposed that EBs are a signature of resistive emergence of undulatory flux tubes, and are produced by magnetic reconnection in bald patches or along their separatrices in the lower chromosphere.

Microflares, also known as subflares or bright points, have been observed and studied for many years (e.g. Svestka 1976; Tandberg-Hanssen & Emslie 1988; Fang et al. 2006b). The typical size of microflares is from several arcseconds to about 20 arcseconds, with a typical lifetime of 10–30 min and a total energy of about 10^{26}–10^{29} erg (e.g. Shimizu et al. 2002; Fang et al. 2006b). Generally speaking, microflares can not only appear in the solar lower atmosphere, but also in the corona, such as in EUV (Emslie & Noyes 1978; Porter et al. 1984) and X-ray bright points (Lin et al. 1984; Krucker et al. 2002; Benz & Grigis 2002). Some observational results imply that the emissions in different wavelengths are coincident. For instance, by using the data of *Yohkoh*/SXT, *SOHO*/EIT and *TRACE*, Berghmans et al. (2001) found that the strongest EUV brightenings were counterparts of soft X-ray microflares. Liu et al. (2004) studied 12 microflares with BBSO/Hα, *RHESSI* images in 3 to 15 keV and *GOES* data, and found all of them are observed in soft X-ray, hard X-ray and Hα. However, the physical relationship between them still needs to be studied further. In this paper, we are mainly interested in those microflares which occur in the chromosphere. To be clear, we call them chromospheric microflares. The most obvious characteristic in the visible spectra of chromospheric microflares is the weak emission at the center of the Hα line, which is not the same as for EBs. This property implies that there should be heating in the upper solar chromosphere. Semi-empirical models of chromospheric microflares indicate that the temperature enhancement is about 1 000–2 200 K (Fang et al. 2006b).

Observations indicate that mass motions exist at or close to the locations of chromospheric microflares. For instance, Shimizu et al. (2002) found that chromospheric ejections were observed in some microflares. Non-thermal properties of some chromospheric microflares are explored in the microwave (e.g. Gary & Zirin 1988; White et al. 1995; Nindos et al. 1999) and hard X-ray emissions (e.g. Nitta 1997; Liu et al. 2004; Qiu et al. 2004). It is also found that some chromospheric microflares are located around or across magnetic polarity inversion lines (Porter et al. 1987; Shimizu et al. 2002; Liu et al. 2004; Fang et al. 2006b). Moreover, observational results suggest that in many cases, emerging flux occurs about 5–30 min before the microflares appear (e.g. Tang et al. 2000;

Shimizu et al. 2002). All these observations imply that magnetic reconnection in the chromosphere could be a plausible mechanism for chromospheric microflares.

Recently, Hinode observations showed the ubiquitous presence of chromospheric anemone jets outside sunspots in active regions (Shibata et al. 2007). Some of them are probably related to EBs or chromospheric microflares. It is believed that they are produced by magnetic reconnection in the lower solar atmosphere.

In order to study EBs and type II white-light flares, Chen et al. (2001) made a two-dimensional numerical MHD simulation and found that magnetic reconnection in the lower solar atmosphere can account for them in many observational aspects, such as lifetime, temperature enhancement, and mass motion. In their simulation, the effect of gravity was ignored and the initial physical parameters were uniform. To improve their results, we make numerical MHD simulations with gravity considered. The influence of different parameters on the results are also studied. The spectral profiles of EBs and chromospheric microflares are calculated with the non-LTE radiative transfer theory and compared with observations. This paper is organized as follows: The numerical method is described in Section 2. The results are given in Section 3, and the discussion and conclusions are given in Section 4.

2 NUMERICAL METHOD

With gravity, ionization and radiation considered, two-dimensional time-dependent compressible resistive MHD equations are taken as follows:

$$\frac{\partial \rho}{\partial t} + \nabla \cdot (\rho \boldsymbol{v}) = 0, \tag{1}$$

$$\rho \frac{\partial \boldsymbol{v}}{\partial t} + \rho(\boldsymbol{v} \cdot \nabla)\boldsymbol{v} + \nabla P - \boldsymbol{J} \times \boldsymbol{B} - \rho \boldsymbol{g} = 0, \tag{2}$$

$$\frac{\partial \boldsymbol{B}}{\partial t} - \nabla \times (\boldsymbol{v} \times \boldsymbol{B}) + \nabla \times (\eta \nabla \times \boldsymbol{B}) = 0, \tag{3}$$

$$\frac{\partial}{\partial t}\Big(\frac{P}{\gamma - 1} + n_{\rm e}\chi_{\rm H} + \frac{\rho v^2}{2}\Big) + \nabla \cdot \Big[\Big(\frac{P}{\gamma - 1} + n_{\rm e}\chi_{\rm H} + \frac{\rho v^2}{2}\Big)\boldsymbol{v}\Big] - \nabla \cdot (P\boldsymbol{v}) - \boldsymbol{E} \cdot \boldsymbol{J} + R - H = 0, \tag{4}$$

where $\nabla = \frac{\partial}{\partial x}\hat{e}_x + \frac{\partial}{\partial y}\hat{e}_y$. The x-axis is along the horizontal direction, and the y-axis is along the vertical direction. The five independent variables are the velocity (v_x, v_y), density (ρ), magnetic flux function (ψ), and temperature (T). We take $\rho = 1.4 m_{\rm H} n_{\rm H}$, where $n_{\rm H}$ is the number density of hydrogen. The magnetic flux function ψ is related to the magnetic field ($\boldsymbol{B}$) by $\boldsymbol{B} = \nabla \times (\psi \hat{e}_z) + B_z \hat{e}_z$. $\boldsymbol{E}$ is the electric field, while $\boldsymbol{J} = \nabla \times \boldsymbol{B}/{\mu_0}^2$ is the current density, and μ_0 is the vacuum permeability. R and H stand for the radiative loss and the pre-heating terms, respectively. The gas pressure $P = 1.1 n_{\rm H} \kappa T$, κ is the Boltzmann constant, and $\chi_{\rm H}$ the ionization potential of hydrogen atoms. Also, $n_{\rm e}$ is the number density of electrons, which is deduced by a modified Saha and Boltzmann formula for a pure hydrogen atmosphere (cf. Gan & Fang 1990)

$$n_{\rm e} = (\sqrt{\phi^2 + 4 n_{\rm H} \phi} - \phi)/2, \tag{5}$$

and

$$\phi = \frac{1}{b_1}\Big(\frac{2\pi m_{\rm e} \kappa T}{h_0^2}\Big)^{3/2} {\rm e}^{-\chi_{\rm H}/\kappa T}, \qquad b_1 = \frac{2T}{T_R} {\rm e}^{\frac{\chi_{\rm H}}{4\kappa T}(\frac{T}{T_R} - 1)},$$

where h_0 is the Planck constant. We take T_R = 6 000 K (cf. Brown 1973).

Radiative loss is important in the lower chromosphere and the upper photosphere. Generally speaking, it should be strictly solved by non-LTE radiative transfer theory. Up to now, however, it has been difficult to deal with in two-dimensional numerical simulations. Instead, Gan & Fang (1990) proposed an empirical formula:

$$R_r = n_{\rm H} n_{\rm e} \alpha(y) f(T), \tag{6}$$

where $\alpha(y)$ and $f(T)$ are functions of y (the height from $\tau_{5000} = 1$ in the photosphere) and the temperature T respectively, and are defined as follows:

$$\alpha(y) = 10^{(2.75\times10^{-3}y - 5.445)} + 2.3738 \times 10^{-4} {\rm e}^{(-y/163)},$$

$$f(T) = 1.547 \times 10^{-23} \Big(\frac{T}{10^4}\Big)^{3/2},$$

where the unit of y is km. The pre-heating rate is given by $H = n_{\rm H}(n_{\rm e}\alpha f)_{t=0}$. In order to perform the numerical simulation, the dimensionless form of the MHD Equations (1)–(4) is used. We take the length scale $L_0 = 2050\,$km, hence the Alfvén transit time $\tau_{\rm A} = L_0/v_{\rm A}$, where $v_{\rm A}$ is the Alfvén velocity. The domain of the numerical simulation is $-1 \leq x/L_0 \leq 1$, $0 \leq y/L_0 \leq 1$. The initial temperature distribution is taken from the quiet-Sun VALC atmospheric model (Vernazza et al. 1981). Using the hydrostatic equilibrium equation, we get the initial number densities of hydrogen atoms ($n_{\rm H}$) as shown in Figure 1.

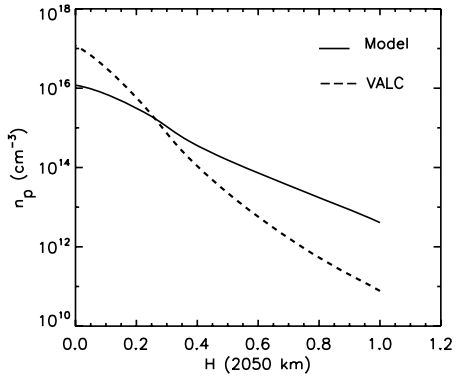

Fig. 1 $n_{\rm p}$ distribution of the initial model.

In order to avoid too wide ranges of hydrogen density and other physical parameters in the atmosphere, we do not include the transition region, where the temperature gradient is very large. Moreover, owing to the omittance of the micro-turbulence and the exact abundance terms, the number density of hydrogen atoms is one order of magnitude smaller than that of the model VALC at the bottom boundary. Nevertheless, our computation can at least simulate the global evolution of magnetic reconnection in the lower solar atmosphere.

The initial magnetic configuration is a force-free field (a current sheet) surrounded by a potential field, which is the same as in Chen et al. (1999). During simulations, an assumed anomalous resistivity (Cramer & Donnelly 1979),

$$\eta/(\mu_0 v_{\rm A} L_0) = \eta_0 \cos[5\pi x/L_0] \cos[10(y/L_0 - h)\pi],$$

is localized in a small region

$$|x|/L_0 \leq 0.1, \qquad |y/L_0 - h_{\rm r}| \leq \Delta h,$$

where $h_{\rm r}$ stands for the height of the reconnection point (X-point) at the y-axis, and Δh the half width of the resistivity region. In the solar atmosphere, the height of the reconnection X-point can indeed increase as the reconnection proceeds (e.g. Takeuchi & Shibata 2001; von Rekowski & Hood 2008). However, here we assume that the height of the X-point is unchanged. The reason is that in our study, we only simulate the reconnection in the lower solar atmosphere. The total height we studied is only 2050 km. During the reconnection process, which we simulate, the height of the X-point does not change very remarkably. This approximation, of course, may have effects on some parameters, such as the lifetime of events. That is one of the reasons why our results are not quantitative but rather qualitative.

Owing to the symmetry about the y-axis, the calculation was performed only in the right half region. The numerical mesh consists of 161×181 points, with 27 points lying within the current sheet. During simulation, we overcome the divergence problem by refining the simulation grid, and computing the middle value by nondimensionalization. Line-tying conditions were applied to the bottom boundary, and symmetry conditions to the left-hand side. The right-hand and the top sides were treated as open boundaries. An equivalent extrapolation was applied to all quantities at the two boundaries, except that at the top, where ρ satisfies $\frac{\partial P}{\partial y} + \rho g = 0$. With gravity, ionization and radiation considered, while heat conduction was omitted, the numerical simulations were performed with a multi-step implicit scheme (Hu 1989; Chen et al. 2001; Xu et al. 2005).

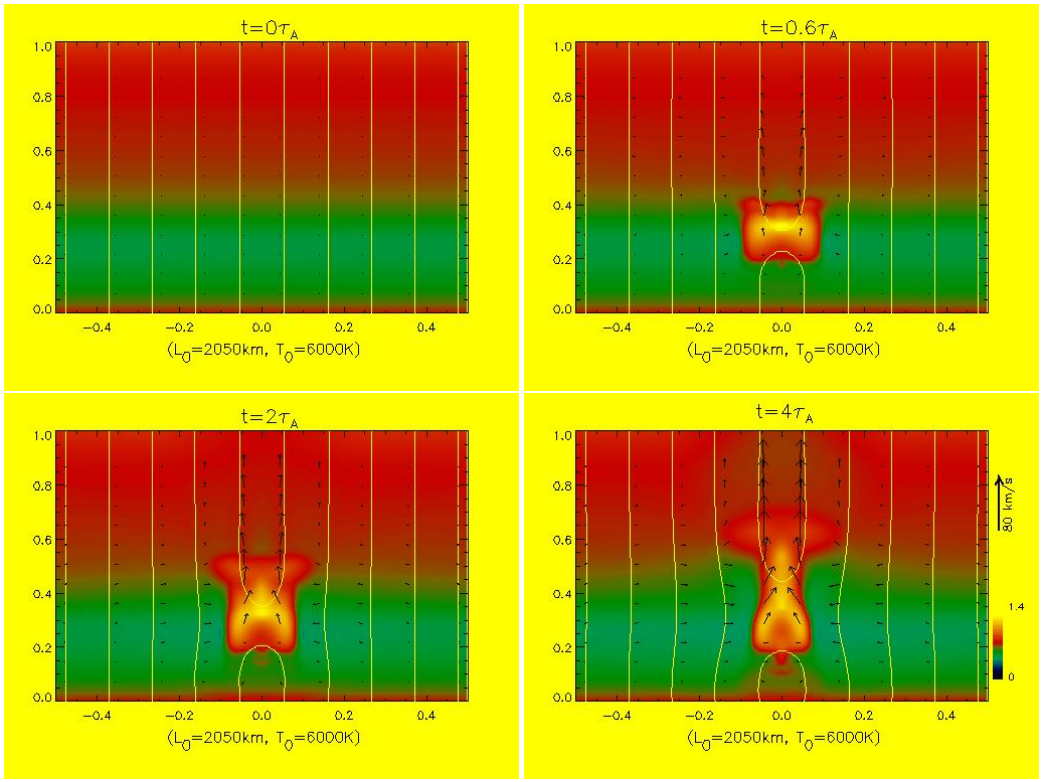

Fig. 2 Temperature distributions (*color scale*), projected magnetic field (*solid lines*) and velocity field (*vector arrows*) at $t = 0\tau_{\rm A}$ and $t = 0.6\tau_{\rm A}$ (*upper panel*) and $t = 2\tau_{\rm A}$ and $t = 4\tau_{\rm A}$ (*lower panel*).

3 NUMERICAL RESULTS

3.1 Dynamic Process

Considering gravity, ionization and radiation, we study magnetic reconnection in the upper photosphere and the chromosphere with different parameters, including the intensity of the background magnetic field B_0 taken from 50 G to 150 G, which should involve as much phenomena as possible for qualitative analysis, and the anomalous resistivity η_0 from 1×10^{-4} to 5×10^{-2}, which is about four to five orders of magnitude larger than the classical resistivity (e.g. Kovitya & Cram 1983). In order to study the effect of the reconnection X-point heights, we take $h_{\rm r}$ = 400 km and 1200 km to represent the upper photosphere and the chromosphere respectively. Δh = 300 km and 800 km have been chosen for the two cases respectively. Figure 2 gives an example of the evolution of magnetic reconnection with $h_{\rm r}$ = 400 km and B_0 = 75 G. In the figure, colors stand for the temperature, solid lines for magnetic field and arrows for velocity. The top-left panel shows the initial condition, while the others correspond to the result at different times. It is noticed that for different background magnetic fields and X-point heights, there are different Alfvén time scales, which are listed in Table 1.

Table 1 Alfvén Time Scales $\tau_{\rm A}$

B_0(G)	$\tau_{\rm A(400\,km)}$ (s)	$\tau_{\rm A(1200\,km)}$ (s)
50	360	58
75	240	39
100	180	29

Our results indicate that the evolution process is as follows: when the anomalous resistivity sets in, two symmetrical convergent inflows move toward the resistivity region. At the same time, two jets are ejected vertically. Due to the lower density in the upper part of the atmosphere, the velocity of the upward jet is larger than that of the downward jet. The reconnected field lines below the X-point pile up due to the line-tying effect at the bottom boundary, forming the closed magnetic loop system which rises slowly. When the loop system moves close to the resistivity region, it hinders the reconnection inflow, slowing the magnetic reconnection process. Compared to the case of the uniform initial atmosphere (Chen et al. 2001), the reconnection in our case can continue longer.

3.2 Parameter Dependence

Figure 3 displays the temperature distributions when the reconnection rate R, defined as the closing rate of the magnetic flux $d\psi/dt$ at the X-point (Forbes & Priest 1983; Chen et al. 1999), is around the maximum for different background magnetic fields when the X-point is at the height of 400 km (a) and 1200 km (b). When magnetic reconnection takes place and the X-point is at the height of 400 km, it is found that the range of temperature enhancement is from 500 K to 1740 K. When the X-point is at the height of 1 200 km, the temperature enhancement is from 930 K to 2320 K. Our results indicate that the temperature enhancement increases with the background magnetic field.

Figure 4 shows the temperature distributions at the time of the reconnection being maximum for different values of η_0 when the X-point is at the height of 400 km (a) and 1200 km (b). Figure 4 demonstrates that the temperature enhancement increases with η_0. This is because the Joule dissipation is the main heating mechanism in our numerical simulation.

We studied the behavior of the magnetic reconnection rate, R, for the two parameters. Figure 5 shows the evolution of R with different background magnetic fields when the X-point is at the height of 400 km (a) and 1200 km (b). It is clear that the maximum of the magnetic reconnection rate is almost not related to the background magnetic field, but the relaxation of the rate is slower for the stronger magnetic field.

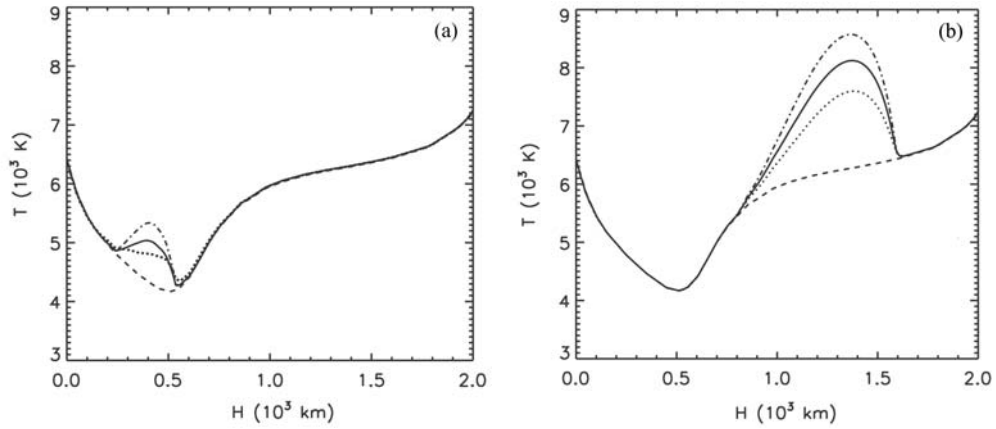

Fig. 3 Temperature distribution resulting from different background magnetic fields. The dashed lines represent the initial temperature distribution in our model, which is the same as that of the quiet-Sun atmospheric model VALC. The background magnetic fields are 50 G (*dotted lines*), 75 G (*solid lines*) and 100 G (*dash-dotted lines*), respectively. The X-point heights along the y-axis, have been taken as 400 km (a) and 1200 km (b). The value of η_0 is 1×10^{-2} (a) and 5×10^{-4} (b).

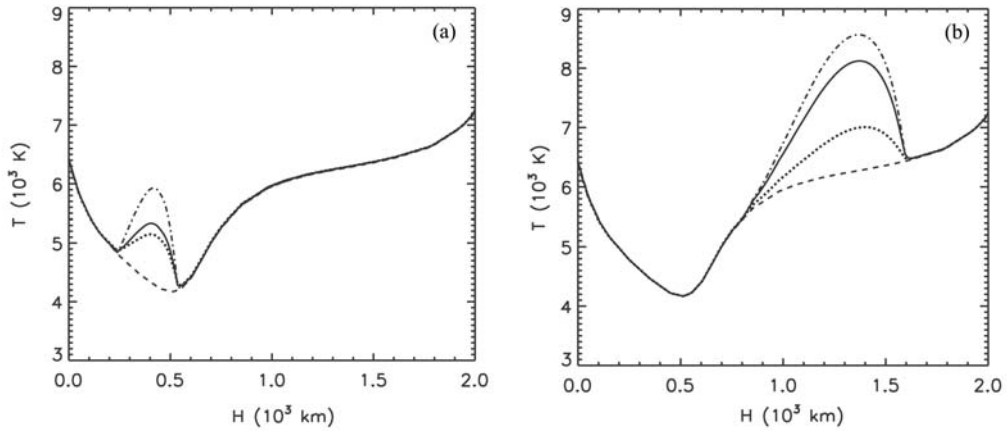

Fig. 4 Temperature distribution resulting from different values of η_0. The X-point of magnetic reconnections is at the height of 400 km (a) and 1200 km (b). The background magnetic field is taken to be 100 G (a) and 75 G (b). The value of η_0 in the panel (a) is 5×10^{-2} (*dash-dotted line*), 1×10^{-2} (*solid line*) and 5×10^{-3} (*dotted line*), respectively, while that in the panel (b) is 1×10^{-3} (*dash-dotted line*), 5×10^{-4} (*solid line*) and 1×10^{-4} (*dotted line*), respectively.

Figure 6 shows the evolution of magnetic reconnection rate with different values of η_0 when the X-point is at the height of 400 km (a) and 1200 km (b). From Figure 6, it can be seen that the maximum of the magnetic reconnection rate increases with η_0.

In order to reproduce the temperature enhancements comparable to the semi-empirical models of EBs (Fang et al. 2006a) and chromospheric microflares (Fang et al. 2006b), we perform a survey of the parameters. The results are shown in Figures 7 and 8. From Figure 7, it can be seen that magnetic reconnection in the upper photosphere can qualitatively explain the temperature enhancement

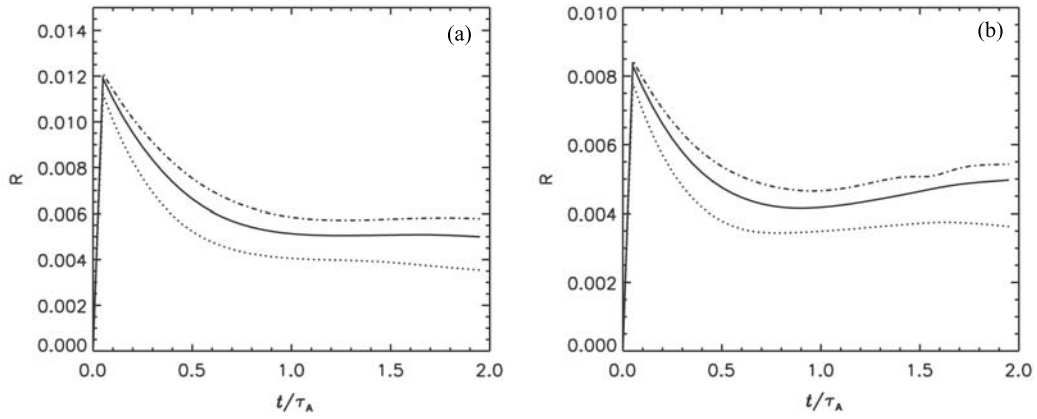

Fig. 5 Evolution of magnetic reconnection rate, R, for different background magnetic fields. Here R is non-dimensional. The X-point of magnetic reconnection is located at the height of 400 km (a) and 1200 km (b). The value of η_0 is taken to be 1×10^{-2} (a) and 5×10^{-4} (b). The background magnetic fields are 50 G (*dotted lines*), 75 G (*solid lines*) and 100 G (*dash-dotted lines*), respectively.

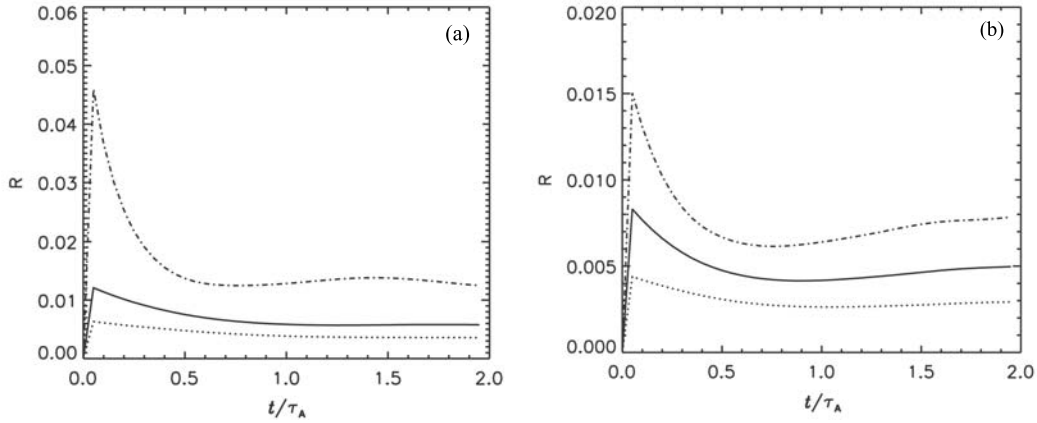

Fig. 6 Evolution of magnetic reconnection rate, R, for different values of η_0. The X-point of magnetic reconnection is located at the height of 400 km (a) and 1200 km (b). The background magnetic field is taken to be 100 G (a) and 75 G (b). The value of η_0 in the panel (a) is taken to be 5×10^{-2} (*dash-dotted line*), 1×10^{-2} (*solid line*) and 5×10^{-3} (*dotted line*), respectively, while that in the panel (b) is 1×10^{-3} (*dash-dotted line*), 5×10^{-4} (*solid line*) and 1×10^{-4} (*dotted line*), respectively.

of EBs (600–1300 K). Figure 8 implies that the temperature enhancement of chromospheric microflares (1 000–2 200 K) could probably be qualitatively produced by magnetic reconnection in the chromosphere. Here we emphasize that the "explanation" is "qualitative," because it is only within our simulation framework, in which there are some assumptions and limitations (see the discussion in Sect. 4).

Based on the results of our numerical simulations, we calculated the spectral excess intensity by using non-LTE radiative transfer theory. The method is similar to that given by Fang et al. (1993). Considering that the initial density distribution in our simulation is different from VALC, which can effect the calculated spectra of Hα and Ca II λ8542 lines, we thus only compare the excess intensities

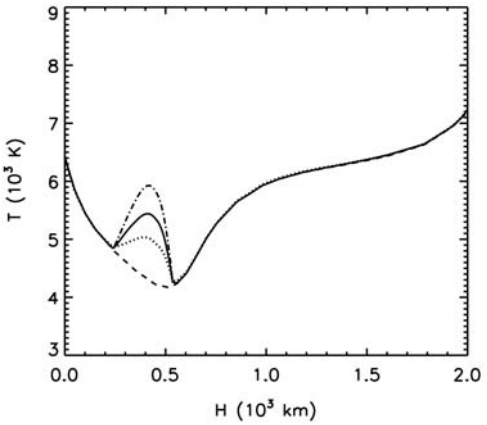

Fig. 7 Temperature distributions comparable to the semi-empirical models of EBs (Fang et al. 2006a) with suitable parameters for magnetic reconnection occurring in the photosphere. The X-point of magnetic reconnection is located at the height of 400 km. The background magnetic field is taken to be 100 G (*dash-dotted line*) and 75 G (*solid line* and *dotted line*). The value of η_0 is taken to be 5×10^{-2} (*dash-dotted line* and *solid line*) and 1×10^{-2} (*dotted line*).

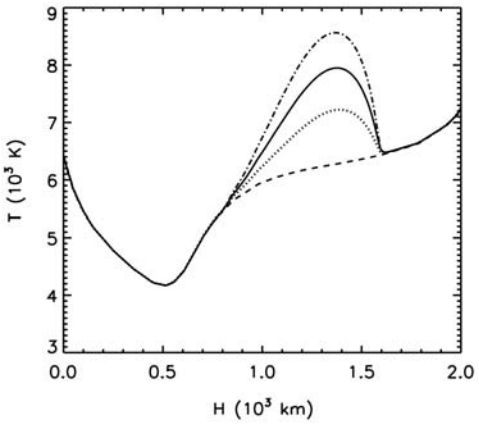

Fig. 8 Temperature distributions comparable to the semi-empirical models of chromospheric microflares (Fang et al. 2006b) with suitable parameters for magnetic reconnection occurring in the chromosphere. The X-point of magnetic reconnection is located at the height of 1 200 km. The background magnetic field is taken to be 75 G (*dash-dotted line*), 50 G (*solid line*) and 100 G (*dotted line*). The value of η_0 is taken to be 1×10^{-3} (*dash-dotted line* and *solid line*) and 1×10^{-4} (*dotted line*).

of the Hα and Ca II lines. That is, we compute the line profiles subtracted from the initial ones. In this case, the effect of the initial density distribution is reduced. The results are shown in Figures 9 and 10, which correspond to the peak time of the magnetic reconnection rate. In Figure 9, the X-point is taken at the height of 400 km, with the background magnetic field being 75 G, and η_0 being 5×10^{-2}. It can be seen that there are two emission bumps in the two wings of both Hα and Ca II λ8542 lines, which are qualitatively similar to the observational results of EBs (Fang et al. 2006a). In Figure 10, the X-point is at the height of 1 200 km, the background magnetic field is 50 G, and the value of η_0 is 1×10^{-3}. The resulting spectra show excess emissions at the center of both Hα and Ca II λ8542 lines, which is qualitatively similar to the observational results of chromospheric microflares (Fang et al. 2006b).

4 DISCUSSION AND SUMMARY

Most of the EBs are located near the longitudinal polarity magnetic inversion lines, and many of them are accompanied by mass motions. Recent semi-empirical models of EBs indicate a temperature enhancement in the lower chromosphere and the upper photosphere (Fang et al. 2006a). Chromospheric microflares have similar characteristics as EBs, but the temperature enhancement is mostly in the chromosphere, as the semi-empirical models indicated (Fang et al. 2006b). All these together with some theoretical work imply that magnetic reconnection in the lower solar atmosphere can produce both EBs (e.g. Hénoux et al. 1998; Ding et al. 1998; Fang et al. 2006a) and chromospheric microflares (e.g. Tandberg-Hanssen & Emslie 1988; Liu et al. 2004; Fang et al. 2006b).

In our simulation, with the X-point height being 400 km, the size of the reconnection region being 300 km and suitable values of the background magnetic field and the anomalous resistivity, the temperature enhancement by magnetic reconnection, as shown in Figure 7, is similar to the observa-

tional results of EBs (e.g. Fang et al. 2006a; Kitai 1983; Georgoulis et al. 2002). For chromospheric microflares, with the X-point height being 1200 km and other suitable parameters, our simulation can also reproduce the temperature enhancement similar to that of observations. Moreover, the computed excess spectral profiles of EBs and chromospheric microflares are also qualitatively similar to the observational ones, as shown in Figures 9 and 10. It should be mentioned that our result can only represent the rise phase of chromospheric microflares, because our simulation was only performed below the transition region. After the upward flow encounters the upper boundary, the simulation cannot produce reliable results. Nevertheless, our results indicate that the heating caused by magnetic reconnection in the lower solar atmosphere can qualitatively give an explanation for the excess intensity of both EBs and chromospheric microflares (at least for the rise phase).

Our simulation can also reproduce some characteristics of EBs and chromospheric microflares, such as the lifetime and the size. Owing to the saturation in magnetic reconnection caused by the line-tying effect, the lifetime of both EBs and chromospheric microflares cannot be very long, as found by Chen et al. (2001). The lifetime depends mainly on the height of the X-point. According to our simulation, when the other conditions are the same, the lower the height is, the shorter the lifetime is. Chromospheric microflares occur in the chromosphere, being generally higher than EBs, so the lifetime of chromospheric microflares is naturally longer than that of EBs. Moreover, we

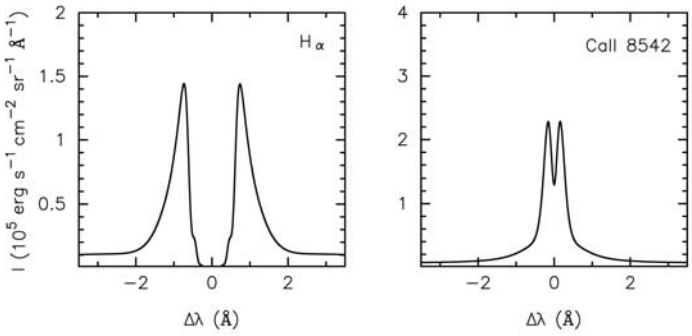

Fig. 9 Computed excess intensity of both Hα and Ca II λ8542 lines based on the X-point located at the height of 400 km. The background magnetic field is taken to be 75 G, with η_0 being 5×10^{-2}.

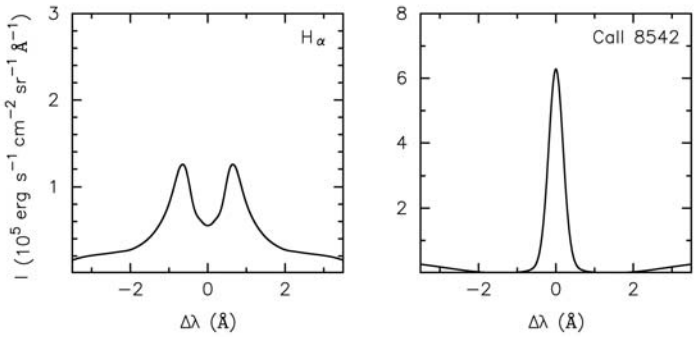

Fig. 10 Computed excess intensity of both Hα and Ca II λ8542 lines based on the X-point located at the height of 1200 km. The background magnetic field is taken to be 50 G, with η_0 being 1×10^{-3}.

also found that the background magnetic field and η_0 have an effect on the lifetime. When the height of the X-point is the same, the bigger the background magnetic field and η_0 are, the shorter the lifetime is. It is worth noting that in the actual solar atmosphere, the X-point can dynamically change as the reconnection proceeds, which was demonstrated by some authors (e.g. Takeuchi and Shibata 2001; von Rekowski & Hood 2008). However, since in our study we only simulate the reconnection in the lower solar atmosphere, the total height we study is only about 2050 km. During the reconnection process, for which we perform the simulation, the height of the X-points does not change so remarkably. We thus can consider that the height of the X-points is almost unchanged. This approximation, of course, may have effects on some parameters, such as the lifetime of events. That is one of the reasons that our results are not quantitative but only qualitative. This is one of the limitations in our numerical simulation.

We would like to mention that in our simulation, we did not study the effect of ionization on the temperature enhancement, though the ionization item is included in our energy Equation (4). As illustrated by Chen et al. (2001, fig. 3), when the ionization effect is included, the heating caused by magnetic reconnection in the upper chromosphere is much less than that not including the ionization effect, because in the former case most of the energy released by magnetic reconnection is converted into ionization potential. Thus, the ionization effect is important and should be considered in the numerical simulation of magnetic reconnection in the chromosphere.

It is worth indicating that our simulations have some limitations. In order to avoid too large a dynamic range of the parameters in the atmosphere, we only used a simple static equilibrium condition and limited the simulation box to be below 2050 km, excluding the temperature transition region, where the temperature gradient is very large. Moreover, owing to the omittance of the micro-turbulence and the exact abundance terms, the number density of hydrogen atoms is one order of magnitude smaller than that of the quiet-Sun atmospheric model, VALC, at the bottom boundary, as seen in Figure 1. Another shortcoming in our study is that we have fixed the height of the X-point, as we have stated in Section 2. All these imply that our simulations cannot reproduce the real observations in details. Further improvement of this work is expected.

As a summary, we give the conclusions as follows:

(1) Our numerical simulations indicate that magnetic reconnection in the solar lower atmosphere can qualitatively explain the temperature enhancement of EBs and chromospheric microflares.
(2) Our simulations can also roughly reproduce the excess Hα and Ca II λ8542 line profiles, which are qualitatively comparable to the observed ones.
(3) EBs and chromospheric microflares with different intensities can be simulated with different parameters, including the strength of the background magnetic field, the anomalous resistivity, the height of the X-point, and the size of the reconnection region. Observations can be used to restrict the range of the parameters.

Acknowledgements We would like to thank Prof. P. F. Chen, who kindly provided many valuable suggestions and help. We greatly appreciate the valuable comments and suggestions from an anonymous referee. This work was supported by the National Natural Science Foundation of China (Grant Nos. 10221001, 10333040, 10403003, 10620150099, 10610099 and 10673004), as well as by the Major State Basic Research Development Program (973 project 2006CB806302).

References

Benz, A. O., & Grigis, P. C. 2002, Sol. Phys., 210, 431
Berghmans, D., McKenzie, D., & Clette, F. 2001, A&A, 369, 291
Brown, J. C. 1973, Sol. Phys., 29, 421
Chen, P. F., Fang, C., & Ding, M. D. 1999, ApJ, 513, 516
Chen, P. F., Fang, C., & Ding, M. D. 2001, ChJAA (Chin. J. Astron. Astrophys.), 1, 176.

Cramer, N. F., & Donnelly, I. J. 1979, PASAu, 3, 367
Dara, H. C., Alissandrakis, C. E., Zachariadis, Th. G., & Georgoulis, A. A. 1997, A&A, 322, 653
Denker, C. 1997, A&A, 323, 599
Denker, C., de Boer, C. R., Volkmer, R., & Kneer, F. 1995, A&A, 296, 567
Ding, M. D., Hénoux J. -C., & Fang, C. 1998, A&A, 332, 761
Emslie, A. G., & Noyes, R. W. 1978, Sol. Phys., 57, 373
Fang, C., Hénoux, J. C., & Gan, W. Q. 1993, A&A, 274, 917
Fang, C., Chen, P. F., & Ding, M. D. 2003, in Proc. 2nd French-Chinese Meeting on Solar Physics, eds. J.-C. Hénoux, C. Fang, & N. Vilmer (Beijing World Publishing), 247
Fang, C., Tang, Y. H., Xu, Z., Ding, M. D., & Chen, P. F. 2006a, ApJ, 643, 1325
Fang, C., Tang, Y. H., & Xu, Z. 2006b, ChJAA (Chin. J. Astron. Astrophys.), 6, 597
Forbes, T. G., & Priest, E. R. 1983, Sol. Phys., 84, 169
Gan, W. Q., & Fang, C. 1990, ApJ, 358, 328
Gary, D. E., & Zirin, H. 1988, ApJ, 329, 991
Georgoulis, M. K., Rust, D. M., Bernasconi, P. N., & Schmieder, B. 2002, ApJ, 575, 506
Hénoux, J. -C., Fang, C., & Ding, M. D. 1998, A&A, 337, 294
Hu, Y. Q. 1989, J. Comput. Phys., 84, 441
Isobe, H., Tripathi, D., & Archontis, V. 2007, ApJ, 657, L53
Kitai, R. 1983, Sol. Phys., 87, 135
Kovitya, P., & Cram, L. 1983, Sol. Phys., 84, 45
Krucher, S., Christe, S., Lin, R. P., et al. 2002, Sol. Phys., 210, 445
Kurokawa, H., Kawakuchi, I., Kunakosi, Y., & Nakai, Y. 1982, Sol. Phys., 79, 77
Lin, R. P., Schwartz, R. A., Kane, S. R., et al. 1984, ApJ, 283, 421
Liu, C., Qiu, J., Gary, D. E., et al. 2004, ApJ, 604, 442
Litvinenko, Y. E. 1999, ApJ, 515, 435
Nindos, A., Kundu, M. R., & White, S. M. 1999, ApJ, 513, 983
Nindos, A., & Zirin, H. 1998, Sol. Phys., 182, 381
Nitta, N. 1997, ApJ, 491, 402
Pariat, E., Aulanier, G., Schmieder, B., et al. 2004, ApJ, 614, 1099
Porter, J. G., Toomre, J., & Gebbie, K. B. 1984, ApJ, 283, 879
Porter, J. G., Moore, R. J., Reichmann, E. J., et al. 1987, ApJ, 323, 380
Qiu, J., Ding, M. D., Wang, H., Denker, C., & Goode, P. R. 2000, ApJ, 544, L157
Qiu, J., Liu, C., Gary, D. E., et al. 2004, ApJ, 612, 530
Shibata, K., Nakamura, T., Matsumoto, T., et al. 2007, Science, 318, 1591
Shimizu, T., Shine, R. A., Title, A. M., et al. 2002, ApJ, 574, 1074
Svestka, Z. 1976, Geophysics and Astrophysics Monographs, 8, 415
Tang, Y. H., Li, Y. N., Fang, C., et al. 2000, ApJ, 534, 482
Tandberg-Hanssen, E., & Emslie, A. G. 1988, The Physics of Solar Flares (Cambridge: Cambridge Univ. Press)
Takeuchi, A., & Shibata, K. 2001, ApJ, 546, L73
Vernazza, J. E., Avrett, E. H., & Loeser, R. 1981, ApJS, 45, 635
von Rekowski, B., & Hood, A. W. 2008, MNRAS, 385, 1792
White, S. M., Kundu, M. R., Shimizu, T., et al. 1995, ApJ, 450, 435
Xu, X. Y., Chen, P. F., & Fang, C. 2005, ChJAA (Chin. J. Astron. Astrophys.), 5, 636
Zachariadis, Th. G., Alissandrakis, C. E., & Banos, G. 1987, Sol. Phys., 108, 227